Acta Pharmacologica Sinica

www.nature.com/aps

ARTICLE

Targeting the ILK/YAP axis by LFG-500 blocks epithelial–mesenchymal transition and metastasis

Cheng-lin Li[1], Juan Li[1], Shu-yuan Gong[1], Meng Huang[1], Rui Li[1], Gui-xiang Xiong[1], Fan Wang[1], Qiu-ming Zou[2], Qi Qi[2] and Xiao-xing Yin[1]

Metastasis is the main cause of mortality in patients with cancer. Epithelial–mesenchymal transition (EMT), a crucial process in cancer metastasis, is an established target for antimetastatic drug development. LFG-500, a novel synthetic flavonoid, has been revealed as a potential antitumor agent owing to its various activities, including modulation of EMT in the inflammatory microenvironment. Here, using a transforming growth factor beta (TGF-β)-induced EMT models, we found that LFG-500 inhibited EMT-associated migration and invasion in human breast cancer, MCF-7, and lung adenocarcinoma, A549, cell lines, consistent with the observed downregulation of YAP activity. Further studies demonstrated that LGF-500-induced suppression of YAP activation was mediated by integrin-linked kinase (ILK), suggesting that the ILK/YAP axis might be feasible target for anti-EMT and antimetastatic treatments, which was verified by a correlation analysis with clinical data and tumor specimens. Hence, our data support the use of LGF-500 as an antimetastatic drug in cancer therapy and provide evidence that the ILK/YAP axis is a feasible biomarker of cancer progression and a promising target for repression of EMT and metastasis in cancer therapy.

Keywords: epithelial–mesenchymal transition; metastasis; LFG-500; YAP; ILK

Acta Pharmacologica Sinica (2021) 42:1847–1859; https://doi.org/10.1038/s41401-021-00655-y

INTRODUCTION

Tumor metastasis is the primary cause of mortality in cancer patients. However, the biology of metastases and the development of druggable targets against tumor metastasis have not been well defined. Epithelial–mesenchymal transition (EMT) enables the escape of cells from primary tumors, promoting the outgrowth of metastases, and it has been established as a target for metastatic treatment in both preclinical and clinical studies, as well as for investigations on antitumor drugs [1]. The most prominent features of EMT are enhanced migration and invasion of cancer cells, which are utilized as two functional parameters to assess the modulation of EMT/metastasis in cancer [2]. During EMT, the levels of the related proteins, N-cadherin and vimentin, are upregulated, whereas E-cadherin and ZO-1 are downregulated, which can be used as markers for EMT assessment at the protein level [3]. Moreover, transcriptional repressors of E-cadherin, such as Snail and Slug, are two markers of EMT at the transcriptional level [4].

Yes-associated protein (YAP), a transcription modulator, is the downstream effector of the Hippo signaling pathway, whose transcriptional activity plays a critical role in EMT and metastasis [5–7]. The transcriptional activity of YAP depends on its nuclear translocation and binding to the transcription factor TEAD, eliciting gene expression signals for EMT [8, 9]. Activation of the Hippo signaling pathway is mediated by a sequential phosphorylation cascade of serine/threonine kinases MST1/2 and Lats1/2, leading to YAP phosphorylation, which blocks YAP nuclear translocation and suppresses its oncogenic activity [10]. Hence, activation of the Hippo signaling pathway is a well-recognized strategy for the management of tumor EMT and metastasis. Various signaling cascades have been demonstrated to regulate the Hippo pathway and YAP activation in cancer [11, 12]. Integrin-linked kinase (ILK), a serine/threonine protein kinase, plays important roles in tumorigenesis, including cell proliferation, angiogenesis, metastasis, and drug resistance [13–15]. The role of ILK in EMT has also been revealed [16–18], which is involved in various mechanisms, such as activation of NF-κB and PI3K/Akt signaling pathways. Recently, ILK has been reported as an upstream inhibitor of the Hippo signaling pathway and has been considered a therapeutic target for cancer treatment [19, 20]. However, the underlying mechanisms of the regulation of the ILK/YAP axis and anticancer compounds targeting the ILK/YAP axis have not been identified.

LFG-500 ($C_{30}H_{32}N_2O_5$), a novel synthetic flavonoid, has been demonstrated as a potential antitumor agent owing to its anti-inflammatory and anticancer effects [21, 22]. We also found that LFG-500 suppresses EMT in lung adenocarcinoma cells within an inflammatory microenvironment [23]. In order to provide more evidence for developing LFG-500 as an anticancer drug, it is necessary to fully elucidate the anti-EMT effects as well as underlying mechanisms of LFG-500 action.

Herein, the anti-EMT activity of LFG-500 was investigated in transforming growth factor beta (TGF-β)-induced EMT model. Mechanistic studies suggested that YAP activity was blocked via

[1]Jiangsu Key Laboratory of New Drug Research and Clinical Pharmacy, Jiangsu Center for the Collaboration and Innovation of Cancer Biotherapy, Xuzhou Medical University, Xuzhou 221004, China and [2]MOE Key Laboratory of Tumor Molecular Biology, Clinical Translational Center for Targeted Drug, Department of Pharmacology, School of Medicine, Jinan University, Guangzhou 510632, China
Correspondence: Qi Qi (qiqikc@jnu.edu.cn) or Xiao-xing Yin (yinxx@xzhmu.edu.cn)
These authors contributed equally: Cheng-lin Li, Juan Li

Received: 22 December 2020 Accepted: 14 March 2021
Published online: 20 April 2021

ILK inhibition by LFG-500, providing more evidence for the ILK/YAP axis as a target for EMT modulation. In addition, the clinical relevance of ILK/YAP axis and cancer metastasis has also been defined, which provides a theoretical foundation for the application of LFG-500 as an antimetastatic drug for cancer treatment.

MATERIALS AND METHODS

Drug and reagents

LFG-500 (99.1% purity) was dissolved in dimethyl sulfoxide (DMSO) and stored at −20 °C. Before each in vitro study, the stock solution was diluted with medium to the required concentrations. The controls were treated with the same amount of carrier solvent (0.1% DMSO) in the corresponding experiments. LFG-500 injection was supplied by Professor Qing-long Guo (China Pharmaceutical University, Nanjing, China) for the in vivo study. The YAP (S127A) plasmid was a kind gift from Professor Xiu-ping Zhou (Xuzhou Medical University, Xuzhou, China). Antibodies against β-actin (AP0060) were obtained from Bioworld (St. Louis Park, MN, USA). Antibodies against E-cadherin (Cat# 3195), N-cadherin (Cat# 13116), vimentin (Cat# 5741), Snail (Cat# 3879), Slug (Cat# 9585), MST1 (Cat# 14946), p-MST1/2 (T183/T180) (Cat# 49332), YAP (Cat# 14074), p-YAP (S127) (Cat# 13008), Lats1 (Cat# 9153), p-Lats1 (T1079) (Cat# 8654), MYPT (Cat# 8574), p-MYPT (T696) (Cat# 5163), Merlin (Cat# 12888), and p-Merlin (S518) (Cat# 13281) were purchased from Cell Signaling Technology (Shanghai, China). Antibodies against ILK (ab52480), ZO-1 (ab96587), and TEAD4 (ab97460) were obtained from Abcam (Cambridge, UK). IRDyeTM800-labeled secondary antibodies were purchased from Rockland Immunochemicals Inc. (Philadelphia, PA, USA). All other reagents were obtained from standard commercial sources.

Cell culture

Human breast cancer MCF-7 and MDA-MB-231 cell lines, human hepatocellular carcinoma HepG2 cell line, human colorectal cancer SW480, and human lung adenocarcinoma A549 cell line were obtained from the Cell Bank of Shanghai Institute of Biochemistry and Cell Biology (Chinese Academy of Sciences, Shanghai, China). MCF-7 and A549 cells were cultured in RPMI-1640 and F-12 media, respectively (Gibco, Invitrogen, Carlsbad, CA, USA). MDA-MB-231 and SW480 cells were cultured in Leibovitz's L-15 medium, and HepG2 cells were maintained in DMEM. The growth medium was supplemented with 10% fetal bovine serum (ExCell Bio, Taicang, Jiangsu, China). Human mammary epithelial MCF10A cells were purchased from the American Type Culture Collection (Manassas, VA, USA) and cultured in a 1:1 mixture of F-12 medium and DMEM (DMEM/F-12), containing 0.1 μg/mL cholera enterotoxin, 10 μg/mL insulin, 0.5 μg/mL hydrocortisone, 20 ng/mL epidermal growth factor, and 5% horse serum. The cells were maintained in a humidified atmosphere under standard culture conditions (95% air, 5% CO_2, and 37 °C).

Spontaneous metastasis mouse model

Male PyMT mice (FVB/N-Tg [MMTV-PyVT] 634Mul/J mice) were obtained from the Model Animal Research Center of Nanjing University (Certificate No. SCXK-[Su] 2010-001) and were randomly bred with homozygous FVB females to obtain female MMTV-PyMT mice. The animals were raised in stainless steel cages under strictly controlled conditions (22 ± 2 °C, 55%–65% humidity, 12 h light/day cycle) and provided ad libitum access to food and water. All animal experimental and surgical procedures were performed according to the Guide for the Care and Use of Laboratory Animals. The study was approved by the Committee on Ethics of Animal Experiments of the Xuzhou Medical University. The surgeries were performed under sodium pentobarbital anesthesia (Sigma-Aldrich, St. Louis, MO, USA) to minimize animal suffering.

Chamber migration and invasion assay

Chamber migration and invasion assays were conducted using a transwell system (10-mm diameter, 8-μm pore-size, polycarbonate membrane; Corning Costar, Cambridge, MA, USA) as previously described [24, 25]. The migrated or invaded cells were stained with 0.5% crystal violet and quantified by manual counting in five randomly chosen fields for each group.

Immunofluorescence and Western blot assay

YAP nuclear translocation in cells was measured using immunofluorescence assay as previously described [26]. For Western blot assay, cells were collected and Western blot analysis was performed according to our previously reported methods [27]. Blots were analyzed using the Odyssey Infrared Imaging System (LI-COR Inc., Lincoln, NE, USA). Polyclonal anti-β-actin was used to verify equal protein loading.

Electrophoretic mobility shift assay (EMSA)

The DNA-binding activities of TEAD4 in nuclear extracts were assessed using EMSA utilizing the EMSA kit (Beyotime Biotechnology, Nantong, China) with biotin-labeled double-stranded TEAD oligonucleotides (Viagene Biotech Inc., Tampa, Florida, USA) according to the manufacturer's recommendations. The forward oligo of the TEAD probe (5′-3′) was TTCGGGACCAGGCCTGGAATG TTTCCACC/biotin/ [28].

Luciferase reporter assay

The 8xGTIIC-luciferase (a gift from Stefano Piccolo, Addgene plasmid #34615) and pRL-SV40 (Renilla luciferase driven by SV40) reporter constructs (Promega, Madison, WI, USA) were transfected into the cells. Luciferase activity was assessed after the cells were treated with TGF-β and various concentrations of LFG-500 (2, 4, or 8 μM) using the Dual-Luciferase® Reporter Assay System (Promega, Madison, WI, USA).

Real-time PCR

Total RNA isolation and real-time PCR were conducted as described previously [29]. The primer sequences synthesized at Sangon Biotech Co., Ltd. (Shanghai, China) were as follows: human ILK, 5′-TCC ACC TGC TCC TCA TCC-3′ (forward) and 5′-CCT CAT CAA TCA TTA CAC TAC GG-3′ (reverse); β-actin, 5′-GGC GGC ACC ACC ATG TAC CCT-3′ (forward) and 5′-AGG GGC CGG ACT CGT CAT ACT-3′ (reverse); mouse ILK, 5′-CAG TGG ATG CAG GGA TGA TGT TCT G-3′ (forward) and 5′-AAA TGG GAC CCT GAA CAA ACA C-3′ (reverse); and β-actin, 5′-AGA GGG AAA TCG TGC GTG AC-3′ (forward) and 5′-CAA TAG TGA TGA CCT GGC CGT-3′ (reverse). Samples were run in the LightCycler 480 Real-Time PCR system (Roche, Basel, Switzerland) at the following conditions: 95 °C for 10 min followed by 50 cycles of 95 °C for 15 s, and 60 °C for 30 s.

In vivo tumor growth and metastasis assay

Female MMTV-PyMT transgenic mice were randomly divided into the following two groups ($n = 7$/group): vehicle control group and 30 mg/kg LFG-500 group. According to a previous study, female MMTV-PyMT transgenic mice promptly develop breast carcinoma at 10 weeks [30]. Thus, the mice were intravenously injected with vehicle or LFG-500 solution every alternate day from week 11 until death. Next, the tumors were collected and weighed. The lungs were rapidly excised, washed, and fixed. The number of metastatic nodules on the lung surface was counted using a dissecting microscope. Histological sections of the lungs were stained with hematoxylin and eosin to verify the presence of malignant nodules and to determine the location and extent of the micrometastatic foci.

Tissue microarray and immunohistochemistry

Breast cancer tissue microarray (TMA) was purchased from Shanxi Alenabio Biotechnology (#BR20837a, Shanxi, China), which

included 1-mm diameter dots of 104 primary breast cancer tissues and 104 corresponding lymph nodes with metastases. All experiments involving samples from human subjects were performed in accordance with relevant guidelines and regulations. The levels of proteins in lung metastatic nodules or TMA specimens were examined using immunohistochemistry, according to previously described methods [31].

Tissue microarray analysis

YAP and ILK staining in TMA specimens were scored independently by two pathologists (who were blinded to the clinical data) using a semiquantitative immunoreactivity score (IRS) as reported previously [32]. Category A documented the intensity of immunostaining on a scale of 0–2, with a score of 0 indicating negative staining, 1 indicating weak staining, and 2 indicating strong staining. Category B documented the percentage of immunoreactive cells on a scale of 1–4, with a score of 1 indicating 0%–25% immunoreactive cells, 2 indicating 26%–50% immunoreactive cells, 3 indicating 51%–75% immunoreactive cells, and 4 indicating 76%–100% immunoreactive cells. IRS was obtained by multiplying scores from categories A and B and ranged from 0 to 8, and the expression was classified as low (IRS, 0–3) or high (IRS, 4–8).

Statistical analysis

Data from at least three independent experiments are expressed as the mean ± SEM. Differences between the groups were evaluated using one-way analysis of variance and Dunnett's post hoc test. For TMA, the associations between YAP or ILK levels and clinicopathologic parameters were evaluated using Fisher's exact test. The comparison of YAP or ILK levels in primary cancer tissues and corresponding metastatic lymph nodes was performed using the Wilcoxon test (grouped). All statistical analyses were conducted using SPSS software (version 19.0; SPSS, Inc., Chicago, IL). Significant differences were represented by $^{*}P < 0.05$ or $^{**}P < 0.01$.

RESULTS

LFG-500 inhibits EMT-associated migration and invasion in cancer cells

Enhanced cellular motility and invasion are prominent features of the EMT in cancer cells. Hence, LFG-500-treated cells were subjected to cell migration and invasion assays. The data showed that, within the noncytotoxic range of concentrations, a high dose of LFG-500 suppressed cell migration and invasion in both MCF-7 and A549 cells (Fig. 1a, b). To validate the role of EMT in the anti-migration and anti-invasion activities of LFG-500, TGF-β-induced EMT cell models were employed [33, 34]. Data showed that TGF-β induced cell motility, which could be reversed by LFG-500 administration (Fig. 1c, d). The transwell invasion assay also showed that LFG-500 suppressed the enhanced invasion in a concentration-dependent manner (Fig. 1e–g). These results indicate that LFG-500 suppresses cell migration and invasion in cancer cells, which may be involved in the repression of EMT.

Identification of the anti-EMT activity of LFG-500 in cancer cells

To further characterize the anti-EMT activity of LFG-500, the key parameters of EMT were examined. Following treatment with TGF-β and various concentrations of LFG-500, cell lysates were collected and subjected to Western blotting. Data showed that TGF-β decreased the expression of epithelial markers ZO-1 and E-cadherin and increased the levels of mesenchymal markers N-cadherin and vimentin in MCF-7 cells. LFG-500 reversed these changes in a dose-dependent manner (Fig. 2a, b). Furthermore, expression of Snail and Slug, known key regulators of EMT [35], was also downregulated by LFG-500, which indicated the repression of EMT by LFG-500 in MCF-7 cells (Fig. 2a, c). Similar effects on the EMT-related proteins of LFG-500 were also observed in A549 cells (Fig. 2d–f). These data demonstrate that LFG-500 inhibits EMT in cancer cells, which may contribute to its antimetastatic effects.

Repression of EMT by LFG-500 is associated with the Hippo–YAP signaling pathway

Because the Hippo signaling pathway and the effector YAP activity play important roles in EMT processes [5–9], we further investigated whether the Hippo signaling pathway was regulated by LFG-500. MCF-7 cells were treated as described above, and cell lysates were analyzed using Western blotting with antibodies against the core kinases of the Hippo signaling pathway. The data indicated that following treatment with LFG-500, the levels of phosphor-MST1/2, phosphor-Lats1, and phosphor-YAP were upregulated in a dose-dependent manner (Fig. 3a, b). It was noted that the levels of total YAP decreased with an increase in phospho-YAP expression in cells treated with increasing concentrations of LFG-500 (Fig. 3a, c). These data indicate that LFG-500 stimulates Hippo signaling, leading to the repression of YAP activity.

YAP oncogenic activity depends on its nuclear translocation and binding to its cotranscription factor TEAD, promoting transcription of genes that contribute to cancer initiation and progression [36, 37]. To identify the role of inhibition of YAP activity in LFG-500-induced EMT repression, we first examined YAP nuclear translocation in MCF-7 cells treated with LFG-500 in the presence and absence of TGF-β. LFG-500 treatment remarkably reversed TGF-β-induced nuclear localization of YAP (Fig. 3d). EMSA results showed that LFG-500 inhibited binding activities in a dose-dependent manner (Fig. 3e). Furthermore, the luciferase reporter assay demonstrated that LFG-500 suppressed the transcriptional activity of the YAP/TEAD complex (Fig. 3f).

To identify the relationship between regression of YAP activity and EMT suppression by LFG-500, a continuously active YAP mutant, YAP (S127A), was employed. Following verification of the activity of YAP (S127A) using EMSA (Supplementary Fig. S1), cells were transfected with vector/YAP (S127A) plasmids and treated with TGF-β/LFG-500 and cell lysates were subjected to Western blotting analysis. Consistent with the regulation of EMT markers described above, cells overexpressing YAP (S127A) remarkably demonstrated an enhanced expression of Snail and vimentin and downregulated expression of E-cadherin (Fig. 3g, h). Notably, in the presence of YAP (S127A), the regulatory activity of LFG-500 on EMT markers was abolished (Fig. 3g, h). The cell migration assay showed that cells expressing YAP (S127A) were resistant to LFG-500, representing a low suppressive effect on TGF-β-induced cell migration (Fig. 3i). The same observations were obtained in A549 cells (Supplementary Fig. S2). Collectively, these results demonstrate that LFG-500 stimulates Hippo signaling and suppresses YAP activity, which is associated with the blockade of EMT in cancer cells.

Involvement of ILK in suppression of EMT by LFG-500 in cancer cells

ILK, an ankyrin repeat-containing serine/threonine protein kinase, has been shown to inhibit the Hippo signaling pathway, which is mediated by inducing phosphorylation of MYPT and downstream Merlin [19, 20]. Hence, we further examined the effects of LFG-500 on the ILK/MYPT/Merlin cascade associated with YAP activity and EMT. Our results showed that TGF-β induced ILK expression, whereas LFG-500 reversed the increase in ILK in a dose-dependent manner (Fig. 4a, b and Supplementary Fig. S3a, b). In parallel with the regulation of ILK, levels of p-MYPT and p-Merlin were downregulated by LFG-500 (Fig. 4a, c), providing an increase in the induction of Hippo signaling and inhibition of YAP activity by LFG-500 as described above. To validate the role of ILK regulation in the anti-EMT effects of LFG-

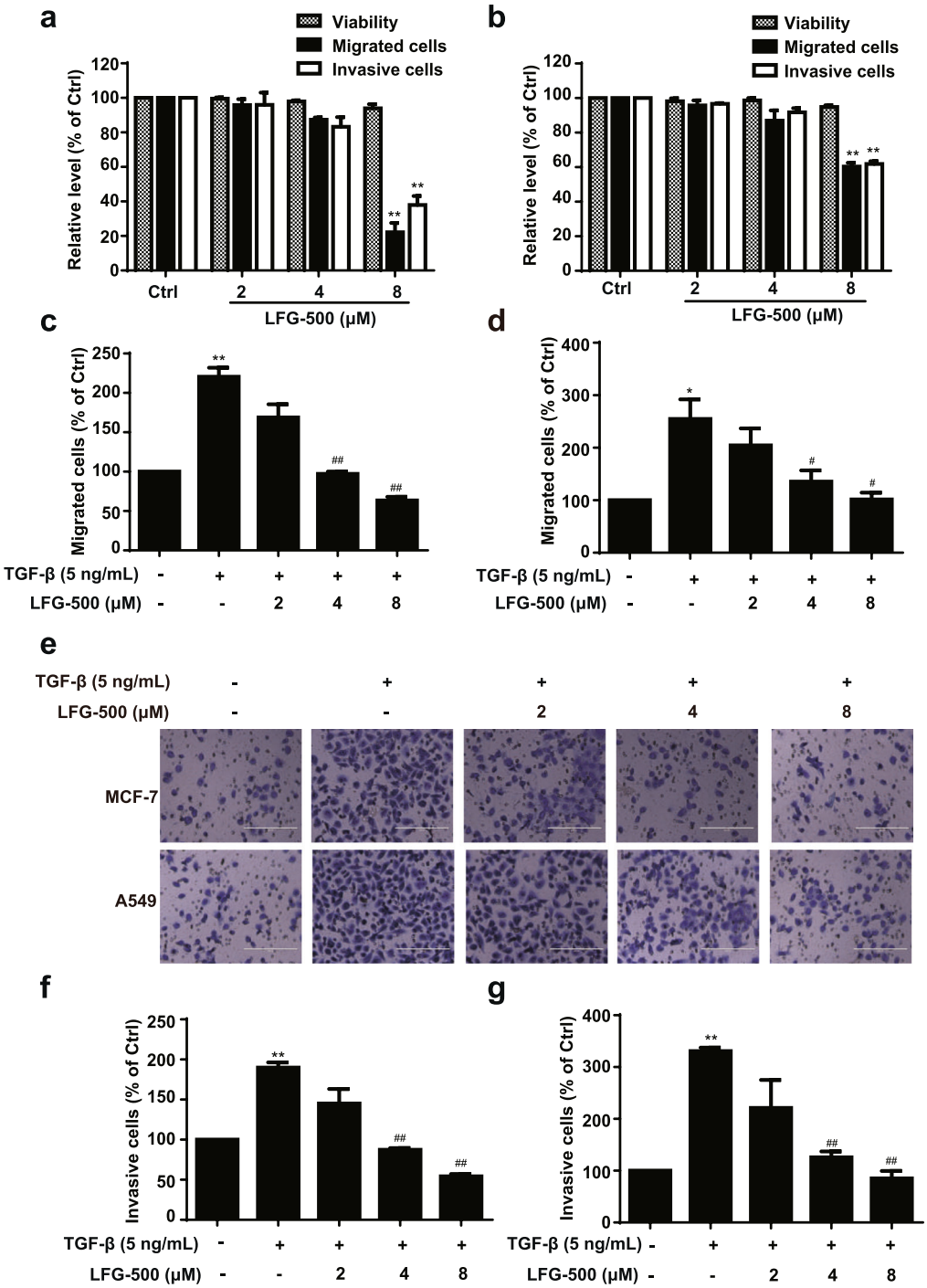

Fig. 1 LFG-500 inhibits the migration and invasion of MCF-7 and A549 cells induced by TGF-β. Effects of LFG-500 on the viability, migration, and invasion of MCF-7 (**a**) and A549 (**b**) cells. Cells were incubated with different concentrations (2, 4, or 8 μM) of LFG-500 for 48 h, then cell viability was examined by trypan blue dye exclusion assay, and migration and invasion ability were evaluated using chamber migration and invasion assay. Effects of LFG-500 on the migration of MCF-7 (**c**) and A549 (**d**) cells induced by TGF-β. Cells were incubated with 5 ng/mL TGF-β and different concentrations (2, 4, or 8 μM) of LFG-500 for 48 h. Migrated cells that passed through the membrane were evaluated by performing crystal violet staining. **e** Effects of LFG-500 on the invasion of MCF-7 and A549 cells induced by TGF-β. Cells were incubated with 5 ng/mL TGF-β and different concentrations (2, 4, or 8 μM) of LFG-500 for 48 h. Invasive cells that passed through the membrane were evaluated by performing crystal violet staining. Invasion images are representative of three independent experiments. Sale bar, 200 μm. Quantification of invasion of MCF-7 (**f**) and A549 (**g**) cells. Data were shown as mean ± SEM. Differences between the groups were evaluated by one-way ANOVA, $n = 3$. $^{*}P < 0.05$ and $^{**}P < 0.01$ represent significant difference compared with control group. $^{\#}P < 0.05$ and $^{\#\#}P < 0.01$ represent significant difference compared with TGF-β group.

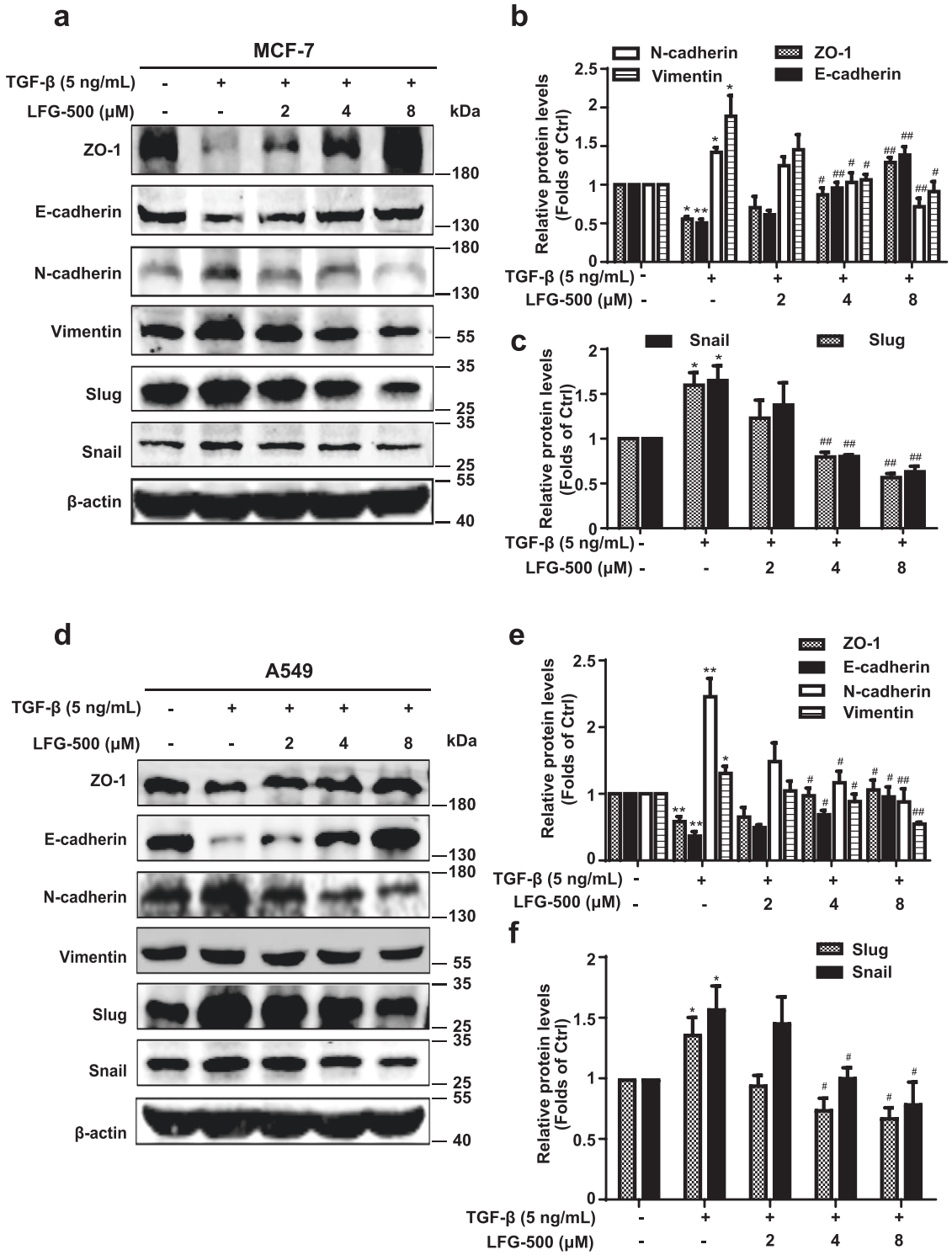

Fig. 2 LFG-500 inhibits TGF-β-induced EMT in MCF-7 and A549 cells. Cells were incubated with 5 ng/mL TGF-β and different concentrations (2, 4, or 8 μM) of LFG-500 for 48 h. **a** Effects of LFG-500 on the levels of EMT-related markers and transcription factors in MCF-7 cells. Levels of ZO-1, E-cadherin, N-cadherin, Vimentin, Slug, and Snail were detected by performing Western blotting with specific antibodies. β-actin was used as a loading control. Densitometric analysis of the EMT-related markers (**b**) and transcription factors (**c**); $n = 3$. **d** Effects of LFG-500 on the levels of EMT-related markers and transcription factors in A549 cells. Western blotting was performed to detect the levels of ZO-1, E-cadherin, N-cadherin, Vimentin, Slug, and Snail. β-actin was used as a loading control. Densitometric analysis of the EMT-related markers (**e**) and transcription factors (**f**); $n = 3$. $^{*}P < 0.05$ and $^{**}P < 0.01$ represent significant difference compared with control group. $^{\#}P < 0.05$ and $^{\#\#}P < 0.01$ represent significant difference compared with TGF-β group.

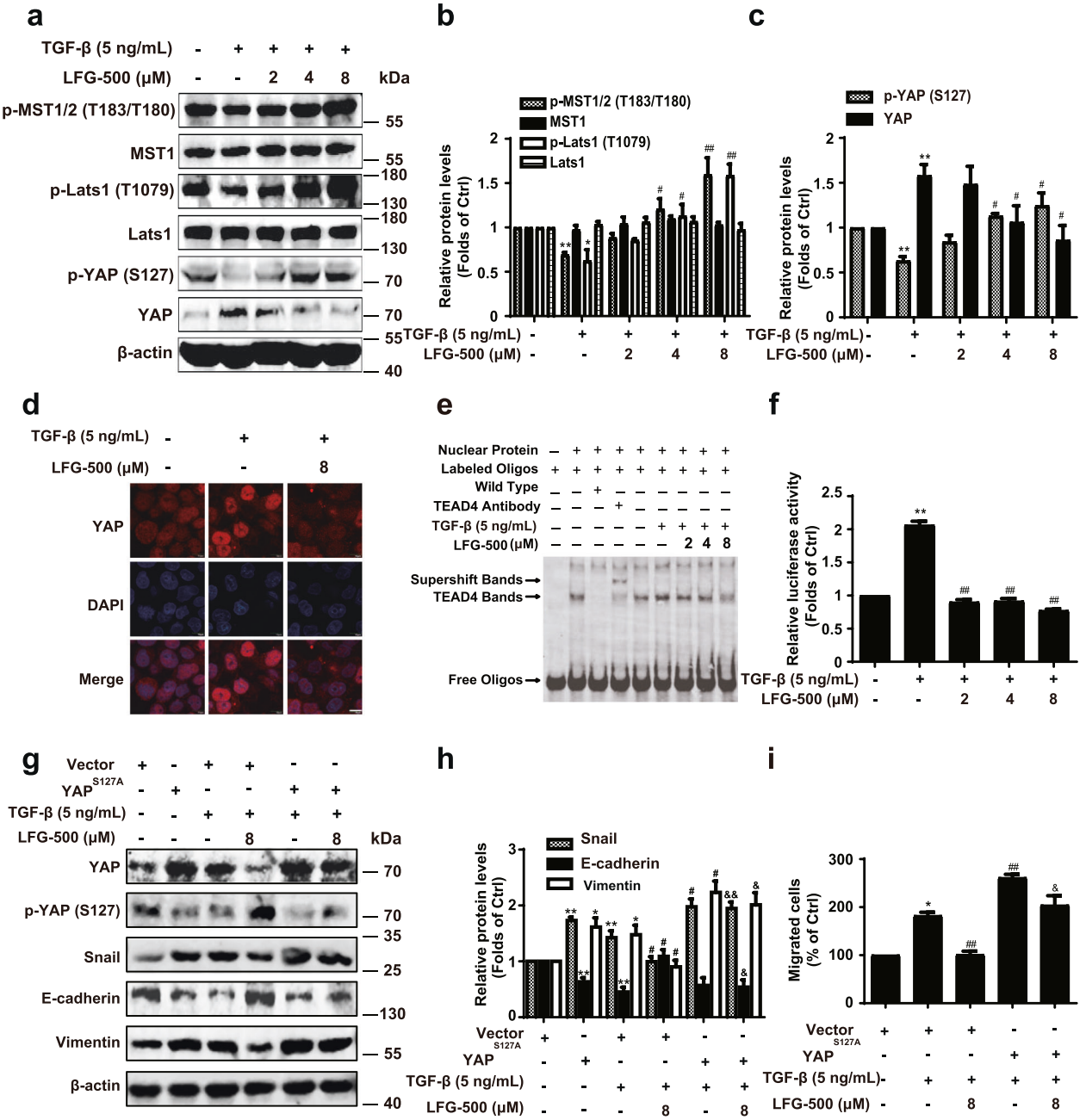

Fig. 3 Repression of EMT by LFG-500 associates with Hippo–YAP signaling pathway. MCF-7 cells were incubated with 5 ng/mL TGF-β and different concentrations (2, 4, or 8 μM) of LFG-500 for 48 h. **a** Effects of LFG-500 on the core kinases of Hippo signaling pathway. Levels of p-MST1/2 (T183/T180), MST1, p-Lats1 (T1079), Lats1, p-YAP (S127), and YAP were detected by performing Western blotting with specific antibodies; β-actin was used as a loading control. **b**, **c** Densitometric analysis of the Western blots; $n = 3$. **d** LFG-500 reverses TGF-β-induced YAP nuclear localization. Cells were immunostained with YAP antibody and DAPI. Representative cells are shown for each treatment (×200). **e** The effects of LFG-500 on DNA-binding activities of TEAD4. The binding activity of nuclear extracts to oligonucleotides was detected by EMSA. A labeled probe containing the area of TEAD binding site was utilized, and the bolt was representative of three experiments. Sale bar, 10 μm. **f** LFG-500 inhibits YAP/TEAD transcription activity in TGF-β-induced MCF-7 cells. The 8xGTIIC-luciferase and pRL-SV40 reporter constructs were transiently transfected into MCF-7 cells. Following different treatment, the promoter activity was detected using the Dual-Luciferase® Reporter Assay System. **g** Transfection with YAP (S127A) plasmid reverses the regulatory effects of LFG-500 on YAP and EMT markers. MCF-7 cells were transfected with vector/YAP (S127A) plasmids and treated with TGF-β/LFG-500 (8 μM). Western blotting was performed to detect the levels of YAP, p-YAP (S127), Snail, ZO-1, and Vimentin; β-actin was used as a loading control. **h** Densitometric analysis of Snail, ZO-1, and Vimentin; $n = 3$. **i** Transfection with YAP (S127A) plasmid reverses the inhibitory effects of LFG-500 on TGF-β-induced migration of MCF-7 cells. The cell migration was evaluated using chamber migration assay. $^{*}P < 0.05$ and $^{**}P < 0.01$ represent significant difference from the control group. $^{\#}P < 0.05$ and $^{\#\#}P < 0.01$ represent significant difference from the TGF-β group. $^{\&}P < 0.05$ and $^{\&\&}P < 0.01$ represent significant difference from the TGF-β and LFG-500 group.

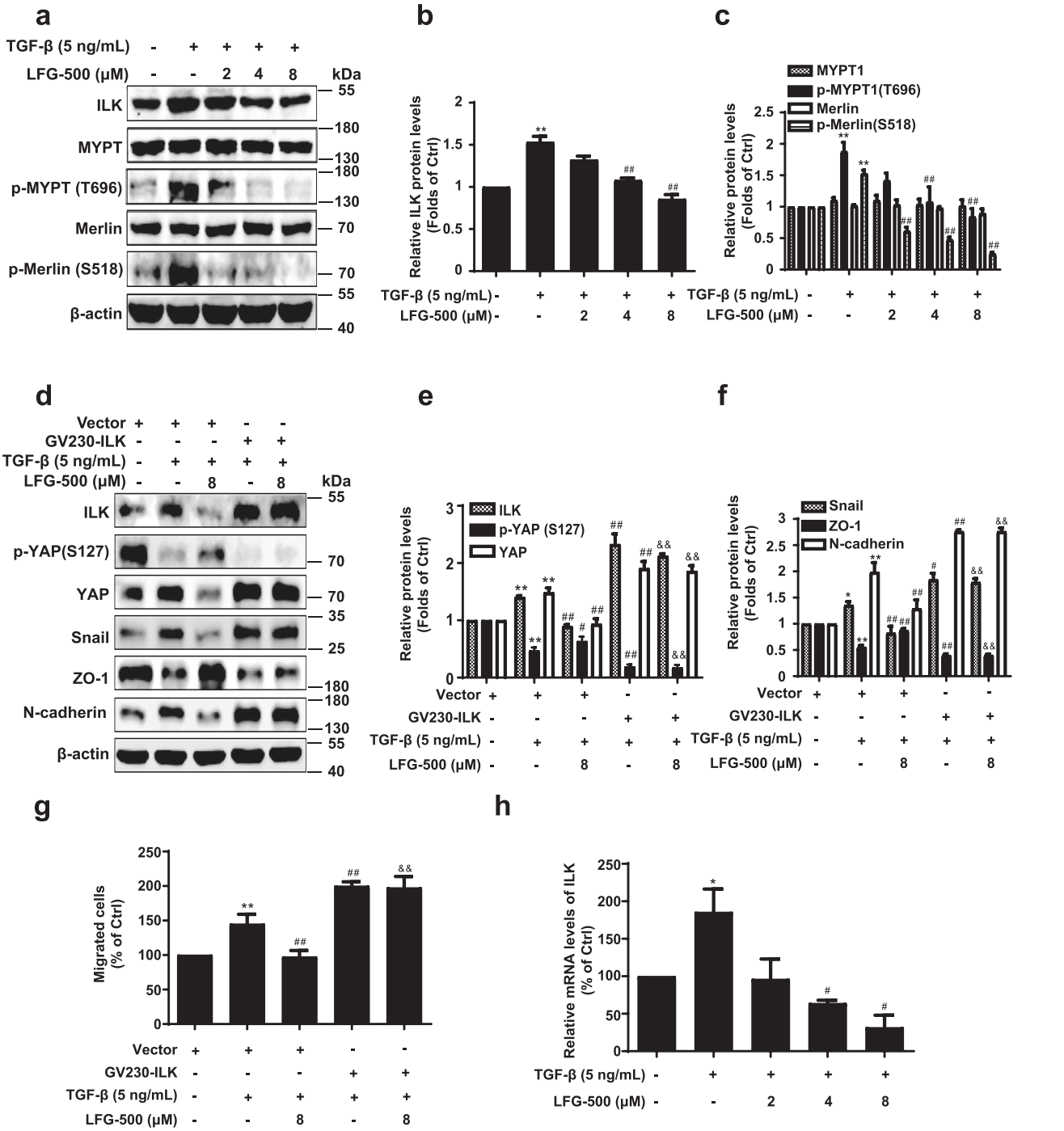

Fig. 4 Involvement of ILK in suppression of EMT by LFG-500. a Effects of LFG-500 on ILK/MYPT/Merlin cascade. Levels of ILK, MYPT, p-MYPY (T696), Merlin, and p-Merlin (S518) were detected by performing Western blotting with specific antibodies; β-actin was used as a loading control. **b**, **c** Densitometric analysis of the Western blots; $n = 3$. **d** ILK overexpression reverses the regulatory effects of LFG-500 on ILK/YAP axis and EMT markers. MCF-7 cells were transfected with vector/GV230-ILK plasmids and treated with TGF-β/LFG-500 (8 μM). Levels of ILK, p-YAP (S127), YAP, Snail, ZO-1, and N-cadherin were detected by performing Western blotting with specific antibodies; β-actin was used as a loading control. **e**, **f** Densitometric analysis of the Western blots; $n = 3$. **g** ILK overexpression eliminates the inhibitory effects of LFG-500 on TGF-β-induced migration of MCF-7 cells. The cell migration was evaluated using chamber migration assay. **h** LFG-500 decreases the mRNA levels of ILK in TGF-β-induced MCF-7 cells. $^{*}P < 0.05$ and $^{**}P < 0.01$ represent significant difference from the control group. $^{\#}P < 0.05$ and $^{\#\#}P < 0.01$ represent significant difference from the TGF-β group. $^{\&\&}P < 0.01$ represents significant difference from the TGF-β and LFG-500 group.

500, cells overexpressing ILK were subjected to LFG-500 treatment. The results showed that ILK overexpression abolished the suppressive effects of LFG-500 on EMT represented by the unchanged levels of EMT markers (Fig. 4d–f and Supplementary Fig. S3c, d), which was verified by migration assay. As shown LFG-500 notably reversed the TGF-β-induced increase of migrated cells. Overexpression of ILK produced stronger effects than those induced by TGF-β, which could not be

abolished by LFG-500 administration (Fig. 4g and Supplementary Fig. S3e).

The above data indicate that protein levels of ILK are downregulated by LFG-500 and that LFG-500 exerts anti-EMT effects by suppressing YAP activity in an ILK-dependent manner in MCF-7 and A549 cells. We also observed similar effects of LFG-500 in MDA-MB-231, HepG2, and SW480 cell lines (Supplementary Fig. S4). Hence, we examined the regulation of ILK by LFG-500 at the mRNA level. Following treatment with various concentrations of LFG-500, mRNA levels of ILK decreased in a concentration-dependent manner (Fig. 4h and Supplementary Fig. S3f). Collectively, these data demonstrate that LFG-500 suppresses ILK mRNA and protein expression, leading to activation of the Hippo signaling pathway and decreased YAP activity, thereby causing its anti-EMT activity.

Effects of LFG-500 on tumor metastasis is associated with regulation of the ILK/YAP axis

As EMT is the key phenotype of cancer metastasis, the MMTV-PyMT mouse model, an aggressive spontaneous breast cancer genetic mouse model with a lung metastatic rate of over 90% [38], was employed to demonstrate the inhibitory effects of LFG-500 on EMT and metastasis in vivo. MMTV-PyMT transgenic mice that developed early carcinoma were treated with LFG-500 (30 mg/kg) and vehicle. LFG-500 treatment remarkably prolonged the survival time of mice (Fig. 5a). In addition, tumor growth was dramatically inhibited by LFG-500, as indicated by the lower tumor weights compared to those in the control group (Fig. 5b). Importantly, LFG-500 remarkably inhibited lung metastasis, represented by fewer numbers and smaller metastatic nodules than those in control mice (Fig. 5c, d).

To validate the regulation of the ILK/YAP axis and EMT by LFG-500 in vivo, lung organs with metastatic nodules were examined using immunohistochemical analysis. Data showed that consistent with the in vitro data, LFG-500 decreased the expression of ILK and YAP, whereas it increased phospho-YAP levels in vivo (Fig. 5e, f). Downregulation of vimentin and upregulation of ZO-1 were also observed in LFG-500-treated mice, which indicated a prominent anti-EMT activity of LFG-500 in vivo. In addition, consistent with the in vitro data, the mRNA levels of ILK were also decreased by LFG-500 treatment (Fig. 5g). Collectively, these results demonstrate that LFG-500 blocks cancer metastasis associated with anti-EMT activity through the modulation of the ILK/YAP axis.

Identification of ILK/YAP axis as a biomarker for diagnosis and prognosis of metastatic cancer

Based on the findings that targeting the ILK/YAP axis confers anti-EMT and antimetastasis activity, the role of the ILK/YAP axis in cancer transformation and progression was further investigated. First, normal human epithelial MCF10A cells transfected with YAP (S127A) and vector were subjected to motility detection. The data showed that YAP (S127A) induced cell migration, suggesting the induction of EMT in MCF10A cells (Fig. 6a). Transfection of the active form of YAP increased the expression of Snail and vimentin and decreased the expression of E-cadherin and ZO-1, demonstrating a prominent role of YAP in inducing EMT (Fig. 6b, c). Next, the role of ILK in YAP-induced EMT was examined. Our results showed that ILK induced YAP activity and cell migration (Fig. 6d, e). Further data showed that ILK notably increased YAP expression in parallel with the induction of EMT, represented by the regulated levels of EMT markers (Fig. 6f, g).

To verify the role of the YAP/ILK axis in cancer progression in vivo, we analyzed the clinical correlation with the Kaplan–Meier plotter database. High expression of ILK and YAP was correlated with poor survival in breast cancer patients (Fig. 7a, b), suggesting that the ILK/YAP axis is a strong prognostic factor associated with poor survival. YAP and ILK levels in primary cancer tissues and corresponding metastatic lymph nodes (YAP for 99 pairs; ILK for 94 pairs) were compared. Data showed that increased YAP levels, especially enhanced nuclear expression of YAP, were observed in metastatic lymph nodes (Fig. 7c and Supplementary Fig. S5). Significant differences in the IRS of ILK expression between metastatic lymph nodes and primary cancer tissues were also detected (Fig. 7d). Additionally, YAP/ILK expression and clinicopathological features of patients with breast cancer at different stages were analyzed. Data showed that YAP and ILK levels in breast cancer tissues were significantly associated with the malignant stage, but not with age (Tables 1 and 2 and Supplementary Fig. S6). Using the clinical samples, the correlation between ILK and YAP expression was analyzed, and the data indicated a positive correlation between ILK and YAP expression in metastatic lymph nodes, but not in primary cancer tissues (Table 3). Taken together, these data demonstrate that ILK/YAP closely correlates with the progression of cancer, as well as the poor prognosis in cancer patients, showing a prominent feature of biomarkers for diagnosis and prognosis of metastatic cancer.

DISCUSSION

In the present study, we provide evidence demonstrating that LFG-500, a small-molecule compound, exerts anti-EMT and antimetastasis effects by targeting the ILK/YAP axis. This finding highlights the role of the ILK/YAP axis in tumor malignancy and cancer metastasis, which was validated by the analysis of clinical specimens from cancer patients. In addition to the biomarker features of the ILK/YAP axis in cancer progression, our data also indicate that the ILK/YAP axis is a promising target for clinical treatment of cancer metastasis.

LFG-500 is a synthetic anti-inflammatory and antitumor flavonoid with improved oral bioavailability [21, 22]. Here, we show that LFG-500 exerts anti-migration and anti-invasion effects in both MCF-7 and A549 cells at concentrations with no cytotoxicity, which are associated with suppression of EMT (Figs. 1 and 2). Further investigations indicated that LFG-500-induced YAP activity confers the anti-EMT effects through downregulation of ILK expression and concurrent activation of the Hippo signaling pathway, which was verified by loss- and gain-of-function studies (Figs. 3 and 4). The anti-EMT effects of LFG-500 were further validated using in vivo studies, showing potent antimetastatic effects in an MMTV-PyMT mouse model (Fig. 5). As an upstream regulator, our data showed that ILK expression was downregulated by LFG-500 at both the protein and mRNA levels. Collectively, our study demonstrates that LEG-500 suppresses EMT through modulation of the ILK/Hippo/YAP signaling pathway. As a pivotal regulator of cancer progression, ILK plays important roles in the regulation of anchorage-dependent cell growth and survival, cell motility and contraction, vascular development, and EMT [39–42]. Here, we found that LFG-500 decreased ILK mRNA levels, suggesting that the transcription of ILK may be regulated by LFG-500. It has been reported that there are multiple transcription factor binding sites within the ILK promoter, including NF-κB [43]. Previously, our group has reported that LFG-500 blocks cancer cell invasion via downregulation of NF-κB-induced matrix metalloproteinase-9 expression [22]. Therefore, it is possible that inhibition of NF-κB contributes to LFG-500-induced downregulation of ILK, which will be comprehensively investigated in our future work. In addition, as SMAD3/4 is the core canonical factor of TGF-β-induced EMT signaling [44] and potential regulator of ILK [45], the effects of LFG-500 on the ILK/YAP axis are associated with SMAD3/4 function, which will be explored in our future work.

With the pharmacological study of LFG-500 to demonstrate its anti-EMT effects, data presented here imply that ILK/YAP axis is a feasible biomarker and target for the management of advanced

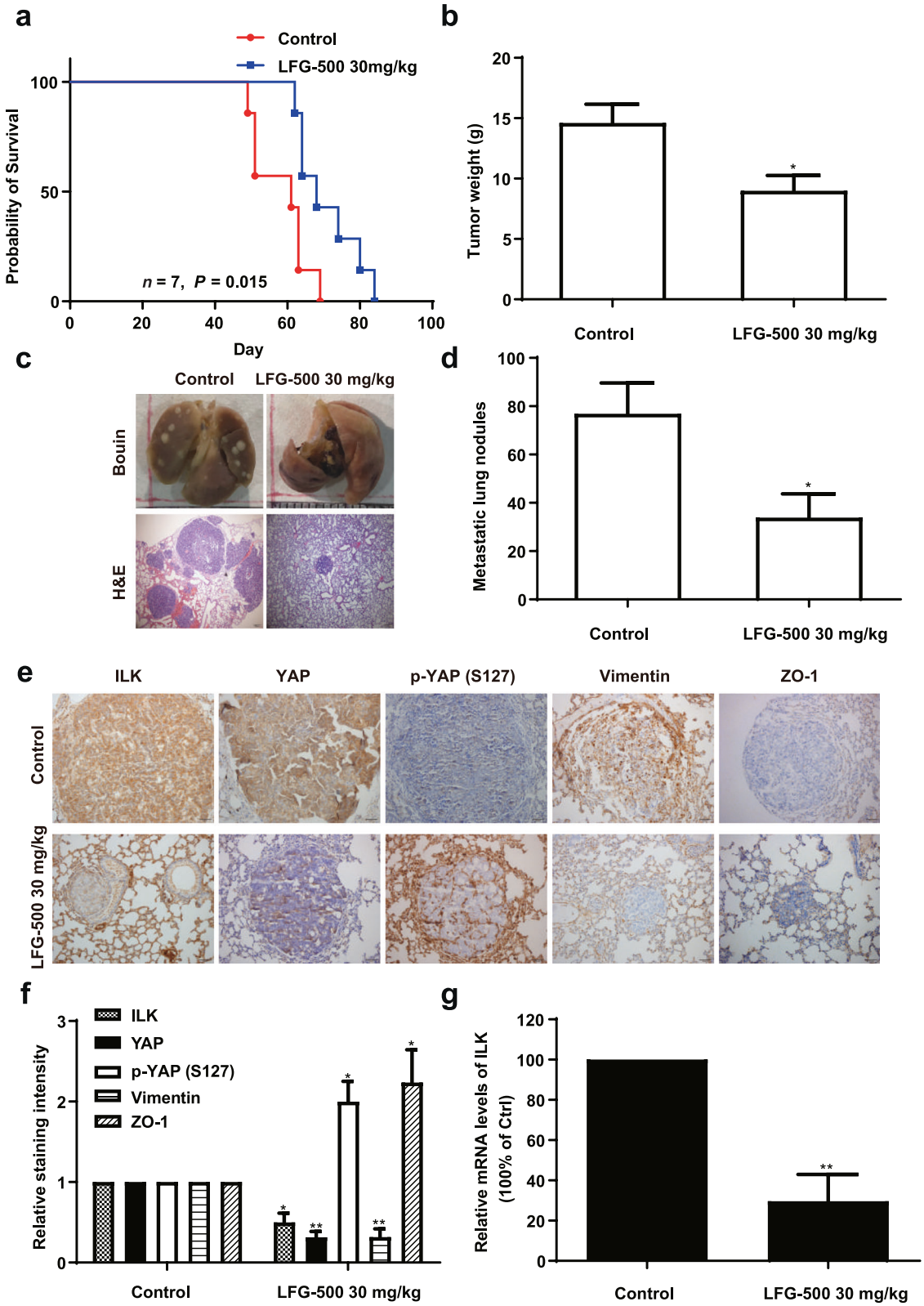

Fig. 5 Effects of LFG-500 on tumor metastasis associated with ILK/YAP axis regulation. The female MMTV-PyMT transgenic mice that developed early carcinoma at week 10 were treated with vehicle or 30 mg/kg LFG-500 every alternate day from week 11 until death. **a** The effects of LFG-500 treatment on the survival time of MMTV-PyMT mice. **b** The tumor weight of different groups. **c** Representative images of lung tissues and H&E-stained metastatic lung nodules. **d** Quantification of the number of metastatic nodules on the lung surface. **e** The levels of ILK, YAP, p-YAP (S127), Vimentin, and ZO-1 in the lung metastatic nodules, as determined by performing immunohistochemical analysis with specific antibodies. **f** Quantitative analysis of the immunohistochemistry assay was performed using ImageJ software, and the results represent the relative staining intensity. **g** LFG-500 decreases the mRNA levels of ILK in tumor. $^{*}P < 0.05$ and $^{**}P < 0.01$ represent significant difference compared with control group.

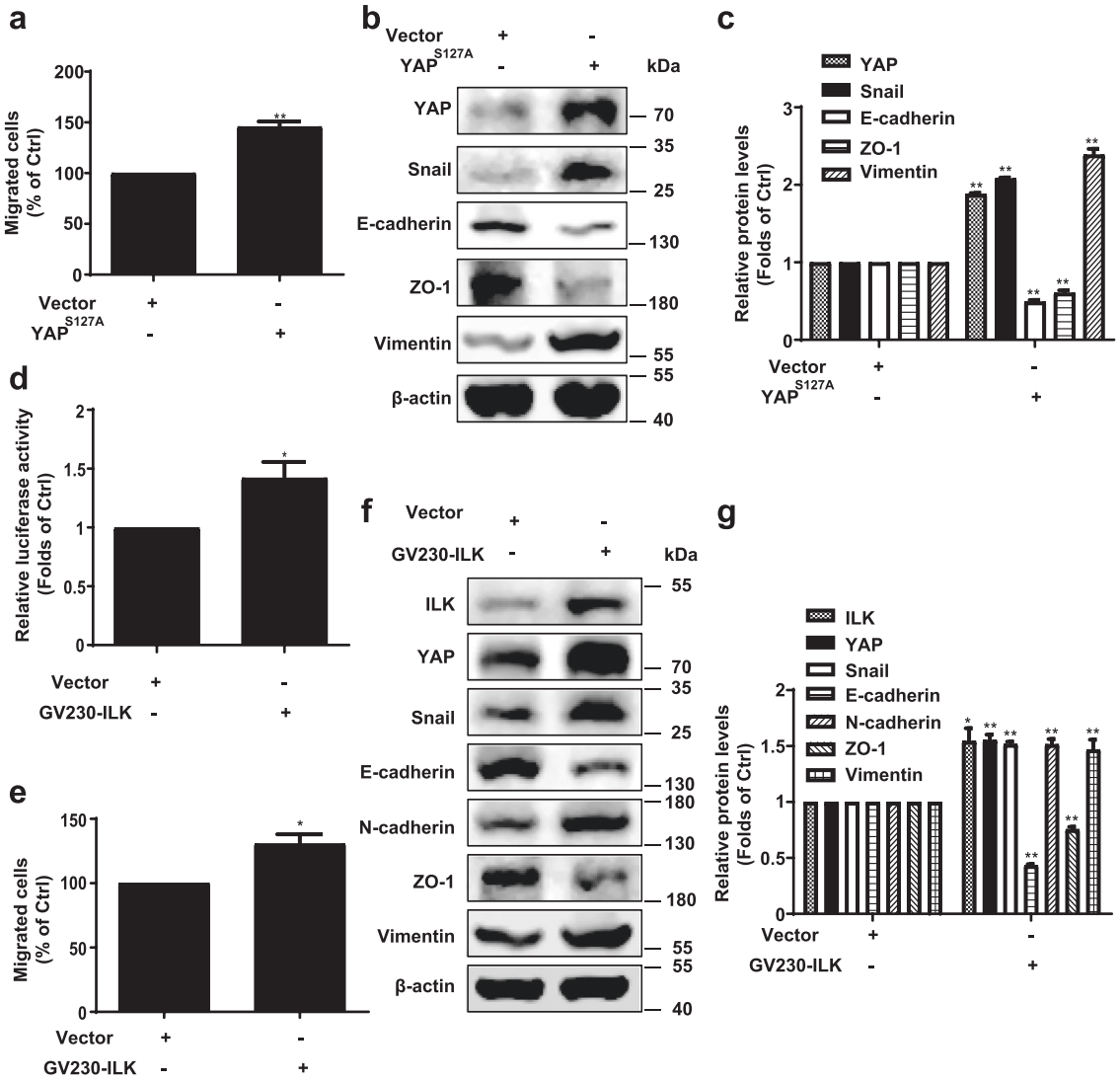

Fig. 6 ILK increases YAP expression in parallel with induction of EMT. Normal human epithelial MCF10A cells were transfected with YAP (S127A) or GV230-ILK plasmids. **a** YAP (S127A) induces cell migration. The cell migration was evaluated using chamber migration assay. **b** Transfection with YAP (S127A) plasmid induces EMT in MCF10A cells. Western blotting was performed to detect the levels of YAP, Snail, E-cadherin, ZO-1, and Vimentin; β-actin was used as a loading control. **c** Densitometric analysis of YAP, Snail, E-cadherin, ZO-1, and Vimentin; $n = 3$. **d** ILK induced YAP transcription activity in MCF10A cells. Following different treatment, the promoter activity was detected using the Dual-Luciferase® Reporter Assay System. **e** ILK overexpression increases migration of MCF10A cells. The cell migration was evaluated using chamber migration assay. **f** Effects of ILK overexpression on the levels of YAP, EMT-related proteins in MCF10A cells. The levels of ILK, YAP, Snail, E-cadherin, N-cadherin, ZO-1, and Vimentin were detected by performing Western blotting with specific antibodies; β-actin was used as a loading control. **g** Densitometric analysis of the Western blots; $n = 3$. $^*P < 0.05$ and $^{**}P < 0.01$ represent significant difference compared with control group.

cancers. The role of the ILK/YAP axis in cancer transformation (EMT) was further validated in MCF10A cells (Fig. 6). Features of the ILK/YAP axis in cancer patient survival, in the relationship of ILK or YAP expression with tumor grades, as well as in the correlation of ILK and YAP expression in the clinic were further analyzed using the Kaplan–Meier plotter database and patient specimens (Fig. 7 and Tables 1–3). The ILK/YAP axis is positively correlated with increased grades of cancer and metastatic stages. However, it is not a biomarker for cancer initiation and formation based on the analysis of transcript expression of ILK and YAP in adjacent normal and tumor tissues in The Cancer Genome Atlas and GSE19804 databases (data not shown). Hence, the ILK/YAP axis is a biomarker of cancer metastasis, and targeting the ILK/YAP axis can be a potential strategy for advanced cancer treatment and antimetastatic drug development.

Since the discovery of ILK in 1996, accumulating evidence has demonstrated ILK as a target for cancer treatment because of its roles in biological processes associated with tumorigenesis [43, 46, 47]. Targeting ILK to block cancer development and progression has been demonstrated using gene knockdown techniques, as well as small molecular inhibitors in vitro and in vivo [48, 49]. However, no compound has been tested in clinical trials worldwide. Therefore, the discovery of new agents targeting ILK for cancer therapy is urgently needed. Flavonoids are natural polyphenols found in plants, fruits, vegetables, teas, and medicinal herbs. In the last decade, the use of phytochemical compounds, including flavonoids, as an interesting and promising strategy for cancer therapy was explored. The anticancer effect of flavonoids is mainly due to their antioxidant and anti-inflammatory activities and their potential to modulate molecular targets and signaling

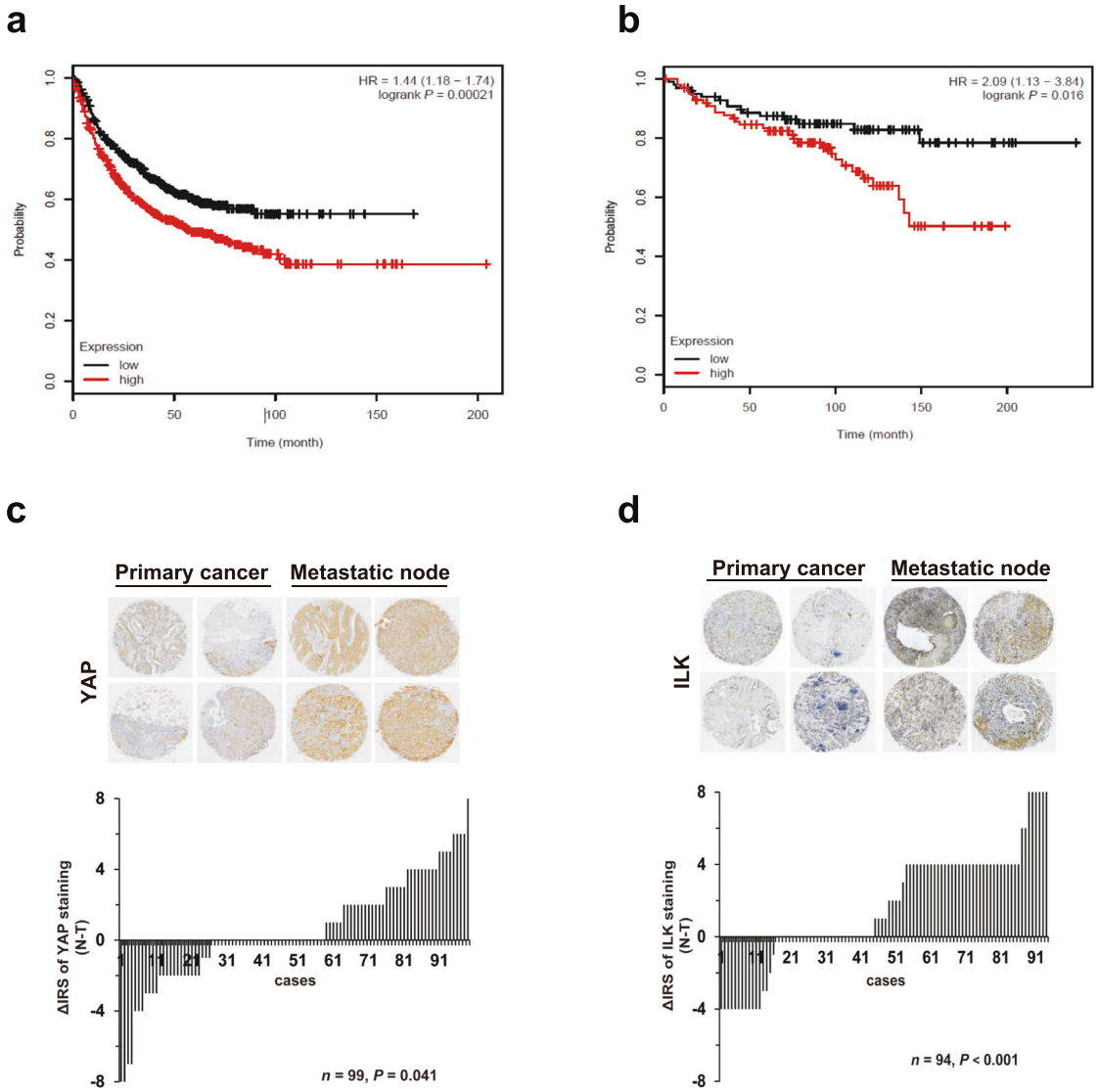

Fig. 7 YAP/ILK axis is a biomarker for diagnosis and prognosis of metastatic cancer. Survival analysis of ILK (**a**) and YAP (**b**) in breast cancer obtained from the Kaplan–Meier Plotter database. Survival was evaluated as RFS (relapse free survival). **c** Enhanced YAP levels were observed in metastatic lymph nodes. Because some samples were lost during antigen retrieval or because relevant cells were absent in the core tissue, YAP levels were examined in 99 pairs that provided both primary cancer tissues and corresponding metastatic lymph nodes. Representative images are shown. Distribution of YAP staining (T tumor tissue, N metastatic lymph nodes, $\Delta IRS = IRS_N - IRS_T$). *P* values were calculated using Wilcoxon test (grouped). **d** Enhanced ILK levels were observed in metastatic lymph nodes. Because some samples were lost during antigen retrieval or because relevant cells were absent in the core tissue, ILK levels were examined in 94 pairs that provided both primary cancer tissues and corresponding metastatic lymph nodes. Representative images are shown. Distribution of ILK staining (T tumor tissue, N metastatic lymph nodes, $\Delta IRS = IRS_N - IRS_T$). *P* values were calculated using Wilcoxon test (grouped).

Table 1. Relationship between YAP expression and clinicopathological features of patients with breast cancer.

Variables	*n* = 99 cases		
	Low[a] (%)	High[a] (%)	*P*[b]
All patients	58 (58.6)	41 (41.4)	
Age, year			0.421
<50	29 (54.7)	24 (45.3)	
≥50	29 (63.0)	17 (37.0)	
Stage			0.030
II	44 (66.7)	22 (33.3)	
III	14 (42.4)	19 (57.6)	

[a]Samples with IRS of 0–3 or with IRS of 4–8 were classified as having high or low YAP expression, respectively.
[b]Two-sided Fisher's exact test.

Table 2. Relationship between ILK expression and clinicopathological features of patients with breast cancer.

Variables	*n* = 95 cases		
	Low[a] (%)	High[a] (%)	*P*[b]
All patients	49 (51.6)	46 (48.4)	
Age, year			0.539
<50	24 (48.0)	26 (52.0)	
≥50	25 (55.6)	20 (44.4)	
Stage			0.019
II	38 (60.3)	25 (39.7)	
III	11 (34.4)	21 (65.6)	

[a]Samples with IRS of 0–3 or with IRS of 4–8 were classified as having high or low ILK expression, respectively.
[b]Two-sided Fisher's exact test.

Table 3. Correlation between ILK and YAP expression in primary cancer and metastatic lymph nodes.

Variables	Low[a]	High[a]	*P*[b]
Primary cancer[c]			0.381
ILK	49	46	
YAP	56	39	
Metastatic lymph node[d]			0.036
ILK	28	69	
YAP	42	55	

[a]Samples with IRS of 0–3 or with IRS of 4–8 were classified as having high or low expression, respectively.
[b]Two-sided Fisher's exact test.
[c]$n = 95$ cases.
[d]$n = 97$ cases.

pathways [50]. In the present study, LFG-500, a novel synthetic flavonoid with improved bioavailability after oral administration [21, 22], has been shown to exert potent anti-EMT and antimetastatic effects in vitro and in vivo via downregulation of ILK, which sheds light on the utilization of flavonoid compounds for cancer targeted therapy.

In summary, we provide compelling evidence demonstrating that LFG-500 suppresses EMT and cancer metastasis through the ILK/YAP axis. Moreover, the role of the ILK/YAP axis positively correlates with the EMT process and cancer malignancy grades. Our findings not only offer a potential candidate against EMT and metastasis, but also delineate features of the ILK/YAP axis as a biomarker and a target for advanced cancer treatment.

ACKNOWLEDGEMENTS

The authors are grateful to Professor Qing-long Guo, who kindly provided LFG-500, to Professor Xiu-ping Zhou for YAP (S127A) plasmid, and to Dr. Hai-ying Li and Dr. Ying Zhang (Department of pathology, Basic Medical Sciences of Xuzhou Medical University) for the assessment of immunohistochemistry. This work was supported by the National Natural Science Foundation of China (grant no. 81402969 and 81973341), supported by the 333 High-level Talents Project of Jiangsu Province, the Six Talent Peaks Project in Jiangsu Province (grant no. 2017-SWYY-075), the Science and Technology Program of Guangzhou (grant no. 202002030010), and the Fundamental Research Funds for the Central Universities (grant no. 21620426), the Science and Technology Innovation Promoting Project of Xuzhou (grant no. KC20066), and the National Demonstration Center for Experimental Basic Medical Science Education (Xuzhou Medical University).

AUTHOR CONTRIBUTIONS

CLL, QQ, and XXY conceived the project, designed the experiments, analyzed the data, and wrote the manuscript. CLL, JL, SYG, MH, and QMZ designed and performed the in vitro experiments. JL, RL, GXX, and FW performed the in vivo study.

ADDITIONAL INFORMATION

Supplementary information The online version contains supplementary material available at https://doi.org/10.1038/s41401-021-00655-y.

Competing interests: The authors declare no competing interests.

REFERENCES

1. Derynck R, Weinberg RA. EMT and cancer: more than meets the eye. Dev Cell. 2019;49:313–6.
2. Zeisberg M, Neilson EG. Biomarkers for epithelial-mesenchymal transitions. J Clin Invest. 2009;119:1429–37.
3. Wang H, Li J, He J, Liu Y, Feng W, Zhou H, et al. Methyl-CpG-binding protein 2 drives the Furin/TGF-beta1/Smad axis to promote epithelial-mesenchymal transition in pancreatic cancer cells. Oncogenesis. 2020;9:76.
4. Mao L, Yang J, Yue J, Chen Y, Zhou H, Fan D, et al. Decorin deficiency promotes epithelial-mesenchymal transition and colon cancer metastasis. Matrix Biol. 2021;95:1–14.
5. Wang Z, Wu Y, Wang H, Zhang Y, Mei L, Fang X, et al. Interplay of mevalonate and Hippo pathways regulates RHAMM transcription via YAP to modulate breast cancer cell motility. Proc Natl Acad Sci USA. 2014;111:E89–98.
6. Wang D, Lin L, Lei K, Zeng J, Luo J, Yin Y, et al. Vitamin D3 analogue facilitates epithelial wound healing through promoting epithelial-mesenchymal transition via the Hippo pathway. J Dermatol Sci. 2020;100:120–8.
7. Shen S, Huang K, Wu Y, Ma Y, Wang J, Qin F, et al. A miR-135b-TAZ positive feedback loop promotes epithelial-mesenchymal transition (EMT) and tumorigenesis in osteosarcoma. Cancer Lett. 2017;407:32–44.
8. Pobbati AV, Hong W. A combat with the YAP/TAZ-TEAD oncoproteins for cancer therapy. Theranostics. 2020;10:3622–35.
9. Zhao W, Li LW, Tian RF, Dong QF, Li PQ, Yan ZF, et al. Truncated TEAD-binding protein of TAZ inhibits glioma survival through the induction of apoptosis and repression of epithelial-mesenchymal transition. J Cell Biochem. 2019;120:17337–44.
10. Qi Q, Li DY, Luo HR, Guan KL, Ye K. Netrin-1 exerts oncogenic activities through enhancing Yes-associated protein stability. Proc Natl Acad Sci USA. 2015;112:7255–60.
11. Fan R, Kim NG, Gumbiner BM. Regulation of Hippo pathway by mitogenic growth factors via phosphoinositide 3-kinase and phosphoinositide-dependent kinase-1. Proc Natl Acad Sci USA. 2013;110:2569–74.
12. Yu FX, Zhao B, Panupinthu N, Jewell JL, Lian I, Wang LH, et al. Regulation of the Hippo-YAP pathway by G-protein-coupled receptor signaling. Cell. 2012;150:780–91.
13. Troussard AA, Costello P, Yoganathan TN, Kumagai S, Roskelley CD, Dedhar S. The integrin linked kinase (ILK) induces an invasive phenotype via AP-1 transcription factor-dependent upregulation of matrix metalloproteinase 9 (MMP-9). Oncogene. 2000;19:5444–52.
14. Wu C, Keightley SY, Leung-Hagesteijn C, Radeva G, Coppolino M, Goicoechea S, et al. Integrin-linked protein kinase regulates fibronectin matrix assembly, E-cadherin expression, and tumorigenicity. J Biol Chem. 1998;273:528–36.
15. Duxbury MS, Ito H, Benoit E, Waseem T, Ashley SW, Whang EE. RNA interference demonstrates a novel role for integrin-linked kinase as a determinant of pancreatic adenocarcinoma cell gemcitabine chemoresistance. Clin Cancer Res. 2005;11:3433–8.
16. Serrano I, McDonald PC, Lock FE, Dedhar S. Role of the integrin-linked kinase (ILK)/Rictor complex in TGFbeta-1-induced epithelial-mesenchymal transition (EMT). Oncogene. 2013;32:50–60.
17. Zhou W, Peng Z, Zhang C, Liu S, Zhang Y. ILK-induced epithelial-mesenchymal transition promotes the invasive phenotype in adenomyosis. Biochem Biophys Res Commun. 2018;497:950–6.
18. Louca M, Zaravinos A, Stylianopoulos T, Gkretsi V. ILK silencing inhibits migration and invasion of more invasive glioblastoma cells by downregulating ROCK1 and Fascin-1. Mol Cell Biochem. 2020;471:143–53.
19. Serrano I, McDonald PC, Lock F, Muller WJ, Dedhar S. Inactivation of the Hippo tumour suppressor pathway by integrin-linked kinase. Nat Commun. 2013;4:2976.
20. Chakraborty S, Njah K, Pobbati AV, Lim YB, Raju A, Lakshmanan M, et al. Agrin as a mechanotransduction signal regulating YAP through the Hippo pathway. Cell Rep. 2017;18:2464–79.
21. Li C, Yang D, Cao X, Wang F, Jiang H, Guo H, et al. LFG-500, a newly synthesized flavonoid, attenuates lipopolysaccharide-induced acute lung injury and inflammation in mice. Biochem Pharmacol. 2016;113:57–69.
22. Li C, Li F, Zhao K, Yao J, Cheng Y, Zhao L, et al. LFG-500 inhibits the invasion of cancer cells via down-regulation of PI3K/AKT/NF-kappaB signaling pathway. PLoS One. 2014;9:e91332.
23. Yang D, Cao X, Wang F, Jiang H, Feng D, Guo H, et al. LFG-500, a novel synthetic flavonoid, suppresses epithelial-mesenchymal transition in human lung adenocarcinoma cells by inhibiting NLRP3 in inflammatory microenvironment. Cancer Lett. 2017;400:137–48.
24. Qi Q, Lu N, Li C, Zhao J, Liu W, You Q, et al. Involvement of RECK in gambogic acid induced anti-invasive effect in A549 human lung carcinoma cells. Mol Carcinog. 2015;54:E13–25.
25. Qi Q, Gu H, Yang Y, Lu N, Zhao J, Liu W, et al. Involvement of matrix metalloproteinase 2 and 9 in gambogic acid induced suppression of MDA-MB-435 human breast carcinoma cell lung metastasis. J Mol Med. 2008;86:1367–77.
26. Li CL, Lu N, Qi Q, Li FN, Ling Y, Chen Y, et al. Gambogic acid inhibits tumor cell adhesion by suppressing integrin beta 1 and membrane lipid rafts-associated integrin signaling pathway. Biochem Pharmacol. 2011;82:1873–83.
27. Li X, Tang X, Su J, Xu G, Zhao L, Qi Q. Involvement of E-cadherin/AMPK/mTOR axis in LKB1-induced sensitivity of non-small cell lung cancer to gambogic acid. Biochem Pharmacol. 2019;169:113635.

28. Qiao Y, Lin SJ, Chen Y, Voon DCC, Zhu F, Chuang LSH, et al. RUNX3 is a novel negative regulator of oncogenic TEAD-YAP complex in gastric cancer. Oncogene. 2016;35:2664–74.
29. Li C, Yang D, Zhao Y, Qiu Y, Cao X, Yu Y, et al. Inhibitory effects of isorhamnetin on the invasion of human breast carcinoma cells by downregulating the expression and activity of matrix metalloproteinase-2/9. Nutr Cancer. 2015;67:1191–200.
30. Lin EY, Jones JG, Li P, Zhu L, Whitney KD, Muller WJ, et al. Progression to malignancy in the polyoma middle T oncoprotein mouse breast cancer model provides a reliable model for human diseases. Am J Pathol. 2003;163:2113–26.
31. Li CL, Zhao YW, Yang D, Yu YY, Guo H, Zhao ZM, et al. Inhibitory effects of kaempferol on the invasion of human breast carcinoma cells by downregulating the expression and activity of matrix metalloproteinase-9. Biochem Cell Biol. 2015;93:16–27.
32. Weichert W, Roske A, Gekeler V, Beckers T, Ebert MPA, Pross M, et al. Association of patterns of class I histone deacetylase expression with patient prognosis in gastric cancer: a retrospective analysis. Lancet Oncol. 2008;9:139–48.
33. Cascione M, De Matteis V, Toma CC, Leporatti S. Morphomechanical alterations induced by transforming growth factor-beta1 in epithelial breast cancer cells. Cancers (Basel). 2018;10:234. https://doi.org/10.3390/cancers10070234.
34. Lu W, Zhang H, Niu Y, Wu Y, Sun W, Li H, et al. Long non-coding RNA linc00673 regulated non-small cell lung cancer proliferation, migration, invasion and epithelial mesenchymal transition by sponging miR-150-5p. Mol Cancer. 2017;16:118.
35. Garg M. Epithelial-mesenchymal transition—activating transcription factors—multifunctional regulators in cancer. World J Stem Cells. 2013;5:188–95.
36. Khandelwal M, Anand V, Appunni S, Seth A, Singh P, Mathur S, et al. Decitabine augments cytotoxicity of cisplatin and doxorubicin to bladder cancer cells by activating hippo pathway through RASSF1A. Mol Cell Biochem. 2018;446:105–14.
37. Meng Z, Moroishi T, Guan KL. Mechanisms of Hippo pathway regulation. Genes Dev. 2016;30:1–17.
38. Cai Y, Nogales-Cadenas R, Zhang QW, Lin JR, Zhang W, O'Brien K, et al. Transcriptomic dynamics of breast cancer progression in the MMTV-PyMT mouse model. BMC Genomics. 2017;18:185. https://doi.org/10.1186/s12864-017-3563-3.
39. Yu YP, Luo JH. Phosphorylation and interaction of myopodin by integrin-link kinase lead to suppression of cell growth and motility in prostate cancer cells. Oncogene. 2011;30:4855–63.
40. Wani AA, Jafarnejad SM, Zhou J, Li G. Integrin-linked kinase regulates melanoma angiogenesis by activating NF-kappaB/interleukin-6 signaling pathway. Oncogene. 2011;30:2778–88.
41. Hannigan GE, Leung-Hagesteijn C, Fitz-Gibbon L, Coppolino MG, Radeva G, Filmus J, et al. Regulation of cell adhesion and anchorage-dependent growth by a new beta 1-integrin-linked protein kinase. Nature. 1996;379:91–6.
42. Kunschmann T, Puder S, Fischer T, Perez J, Wilharm N, Mierke CT. Integrin-linked kinase regulates cellular mechanics facilitating the motility in 3D extracellular matrices. Biochim Biophys Acta Mol Cell Res. 2017;1864:580–93.
43. Zheng CC, Hu HF, Hong P, Zhang QH, Xu WW, He QY, et al. Significance of integrin-linked kinase (ILK) in tumorigenesis and its potential implication as a biomarker and therapeutic target for human cancer. Am J Cancer Res. 2019;9:186–97.
44. Tang C, Mo X, Niu Q, Wahafu A, Yang X, Qui M, et al. Hypomorph mutation-directed small-molecule protein-protein interaction inducers to restore mutant SMAD4-suppressed TGF-beta signaling. Cell Chem Biol. 2020;S2451-9456:30473-6. https://doi.org/10.1016/j.chembiol.2020.11.010.
45. Du M, Wang Q, Li W, Ma X, Wu L, Guo F, et al. Overexpression of FOXO1 ameliorates the podocyte epithelial-mesenchymal transition induced by high glucose in vitro and in vivo. Biochem Biophys Res Commun. 2016;471:416–22.
46. Canel M, Serrels A, Frame MC, Brunton VG. E-cadherin-integrin crosstalk in cancer invasion and metastasis. J Cell Sci. 2013;126:393–401.
47. Rothe K, Babaian A, Nakamichi N, Chen M, Chafe SC, Watanabe A, et al. Integrin-linked kinase mediates therapeutic resistance of quiescent CML stem cells to tyrosine kinase inhibitors. Cell Stem Cell. 2020;27:110.
48. Xing Y, Qi J, Deng S, Wang C, Zhang L, Chen J. Small interfering RNA targeting ILK inhibits metastasis in human tongue cancer cells through repression of epithelial-to-mesenchymal transition. Exp Cell Res. 2013;319:2058–72.
49. Lee SL, Hsu EC, Chou CC, Chuang HC, Bai LY, Kulp SK, et al. Identification and characterization of a novel integrin-linked kinase inhibitor. J Med Chem. 2011;54:6364–74.
50. Hosseinzadeh E, Hassanzadeh A, Marofi F, Alivand MR, Solali S. Flavonoid-based cancer therapy: an updated review. Anticancer Agents Med Chem. 2020;20:1398–414.